



HAL
open science

Light in the Cave: Opal coating detection by UV-light illumination and fluorescence in a rock art context. Methodological development and application in Points Cave (Gard, France)

Marine Quiers, Claire Chanteraud, Andréa Maris-Froelich, Emilie Chalmin, Stéphane Jaillet, Camille Noûs, Sébastien Pairis, Yves Perrette, Hélène Salomon, Julien Monney

► **To cite this version:**

Marine Quiers, Claire Chanteraud, Andréa Maris-Froelich, Emilie Chalmin, Stéphane Jaillet, et al.. Light in the Cave: Opal coating detection by UV-light illumination and fluorescence in a rock art context. Methodological development and application in Points Cave (Gard, France). 2021. hal-03383193v1

HAL Id: hal-03383193

<https://hal.science/hal-03383193v1>

Preprint submitted on 21 Oct 2021 (v1), last revised 14 Jun 2022 (v5)

HAL is a multi-disciplinary open access archive for the deposit and dissemination of scientific research documents, whether they are published or not. The documents may come from teaching and research institutions in France or abroad, or from public or private research centers.

L'archive ouverte pluridisciplinaire **HAL**, est destinée au dépôt et à la diffusion de documents scientifiques de niveau recherche, publiés ou non, émanant des établissements d'enseignement et de recherche français ou étrangers, des laboratoires publics ou privés.

Light in the Cave: Opal coating detection by UV-light illumination and fluorescence in a rock art context

Methodological development and application in Points Cave (Gard, France)

Marine Quiers ^{a,*}, Claire Chanteraud ^{b,c}, Andréa Maris-Froelich ^a, Émilie Chalmin-Aljanabi ^c, Stéphane Jaillot ^c, Camille Noûs ^e, Sébastien Pairis ^d, Yves Perrette ^{c,b}, Hélène Salomon ^c, Julien Monney ^c

^aLaboratoire Commun SpecSolE, Envisol – CNRS - Univ. Savoie Mont Blanc, Chambéry, 73000, France

^bMissouri University Research reactor - University of Missouri 65203 Columbia MO

^cEDYTEM UMR5204, CNRS, Univ. Savoie Mont Blanc, Chambéry, 73000, France

^dUniv. Grenoble Alpes, CNRS, Grenoble INP, Institut Néel, Grenoble, 38000, France

^eLaboratoire Cogitamus, 1 ¾ rue Descartes, Paris, 75005, France

* Corresponding author: m.quiers@envisol.fr

Abstract

Silica coatings developed on rock art walls in Points Cave question the access to pictorial matter specificities (geochemistry and petrography) and the rock art conservation state in the context of pigment studies. However, classical *in situ* spectroscopic techniques appear unsuccessful to identify these coatings, which also prevent pigment characterization. In this study, we propose using a UV fluorescence method for opal coating detection based on the fluorescence specificities of uranyl-silica complexes composing these deposits. A coupling of spectral identification using UV laser-induced fluorescence spectroscopy with UV illumination was performed on samples and μ -samples from the Points Cave rock art site. The well-defined peaks observed in fluorescence emission spectra due to uranyl ions validate opal detection and its correspondence with green fluorescence observed under UV light at micro- and macroscopic scales. *In situ* optical measurements under UV illumination reveal the presence of opal coating, especially on rock art walls in Points Cave. Opal occurrence and repartition observations provide the first insights into Points Cave wall evolution and chronological constraints linked to opal coating development. Regarding the strong interactions with pigment suggested by

35 multiscale observations of samples and μ -samples, the impact of the presence of opal coating on
36 Points Cave rock art conservation quality is questioned. Thus, by developing a specific and non-
37 destructive characterization method for opal coatings, this study opens up a new approach for the
38 study of decorated wall taphonomy and proposes utilizing mineralization both as markers of the
39 natural history of caves and as an indication for their occupation by ancient human groups.

40

41 **Keywords:** Silica coating, uranyl, UV fluorescence, *in situ* detection, rock art cave, Quaternary,
42 archaeology, Ardèche, France, optical methods

43

44

45

46 **1. Introduction**

47

48 Natural activity in caves, mostly weathering, transforms the physical, chemical and mechanical
49 conditions on the surface of the walls (Bassel, 2017; Chalmin *et al.*, 2018). Thus, the traces of all these
50 transformations (environmental input) can be a source of information regarding natural and
51 anthropological events on the wall surface, such as drawing and painting realizations, cave
52 environment evolution, and human attendance in the cave (Sadier, 2013; Pons-Branchu *et al.*, 2014;
53 Quilès *et al.*, 2015; Quing-Feng *et al.*, 2017; Garate *et al.* 2018; Valladas *et al.*, 2017; Money & Jaillet,
54 2019).

55

56 Among the taphonomic processes impacting rock art pictorial matter, mineral-coating formation as
57 weathering products is well described in rock art research (Huntley, 2012). Silica rich amorphous
58 deposits, also called silica skins, have been observed at different cave and open-air parietal sites
59 (Watchman, 1990; Aubert *et al.*, 2004; Aubert *et al.*, 2012; Huntley, 2012). Thus, studies have
60 suggested both a positive and negative impact on rock art conservation due to opal coating

61 development. Indeed, the strong interaction suspected with haematite pigments has been suggested as
62 an element of conservation enhancement, notably compared with other pigments (Watchman, 1990).
63 However, some authors have also observed exfoliation processes of silica skins, which could play a
64 role in rock art weathering (Aubert *et al.*, 2004; Green *et al.*, 2017). To our knowledge, there is still no
65 clear answer on the role of silica coatings as conservation factors of pictorial matter. In addition to this
66 conservation issue, silica skins have been proposed as tools for indirect dating of parietal art,
67 especially in the case of inorganic pictorial matter (Aubert *et al.*, 2004; Aubert *et al.*, 2012). Indeed,
68 this mineral phase is known to be enriched in uranyl ions, but the U-Th dating application remains
69 hypothetical due to silica skin thickness and absence of stratigraphy, which complicate both sampling
70 and measurement reliability (Green *et al.*, 2017).

71

72 Thus, even if silica skin characterization represents a key issue in the rock art context, it remains
73 difficult to identify and characterize, especially with non-invasive techniques. Currently, the use of *in*
74 *situ* spectroscopic techniques in rock art studies is increasing, as these methods can provide
75 information on both pictorial matter and pigment environments (substrate, deposits, concretions, etc.).
76 The portability and decreasing cost of instruments coupled with the rapidity and the non-destructive
77 character of analyses have led to a quasi-systematic use of these techniques in recent rock art studies
78 (Huntley, 2012). However, amorphous silica characterization, even in the rock art context, is generally
79 based on laboratory observations such as SEM or XRD analyses (Watchman, 1990; Gaillou *et al.*,
80 2008; Garcia-Guinea *et al.*, 2013; Huntley *et al.*, 2015; Green *et al.*, 2017). In addition, the signal of
81 pictorial matter acquired with portable spectroscopic techniques could be impacted by the presence of
82 silica skins, as observed by Huntley (2012) in the case of pXRF measurements.

83

84 In this paper, we propose a new method for the *in situ* detection and characterization of amorphous
85 silica in a rock art context based on UV laser-induced fluorescence (LIF). Indeed, uranyl fluorescence
86 characteristics under UV light are well known and have been observed in silica mineralization,
87 especially in opal (deNeufville *et al.*, 1981; Gorobets *et al.*, 1977; Fritsch *et al.*, 2001; Gaillou *et al.*,

88 2008). Thus, UV spectroscopy presents the same advantages as other portable spectroscopic
89 techniques, but the bright green fluorescence and the specific spectral features displayed by uranyl
90 ions enable the targeted identification of opal coatings. To our knowledge, only one study has reported
91 opal detection in caves using optical methods based on UV techniques (Garcia-Guinea *et al.*, 2013),
92 and no study has applied UV spectroscopic methods in a rock art context for opal identification. Here,
93 we propose a methodological development based on laboratory and field experiments to validate the
94 use of *in situ* UV techniques for opal detection in a rock art context by coupling *in situ* optical and
95 spectroscopic analyses to obtain multiscale information.

96

97 This study was performed in Points Cave (Aiguèze, Gard, France), which contains an important spread
98 of opal coating on the cave walls. In this approach, Points Cave perfectly illustrates the importance of
99 environmental input characterization in the study of rock art. The advantage of this site is given by the
100 presence of colouring flakes falling from cave walls, allowing transport, μ -sampling and analysis in
101 the laboratory. Analysis of these coloured flakes allows us to identify and measure the environmental
102 input, which modifies and obscures the identification of pictorial matter characteristics.

103

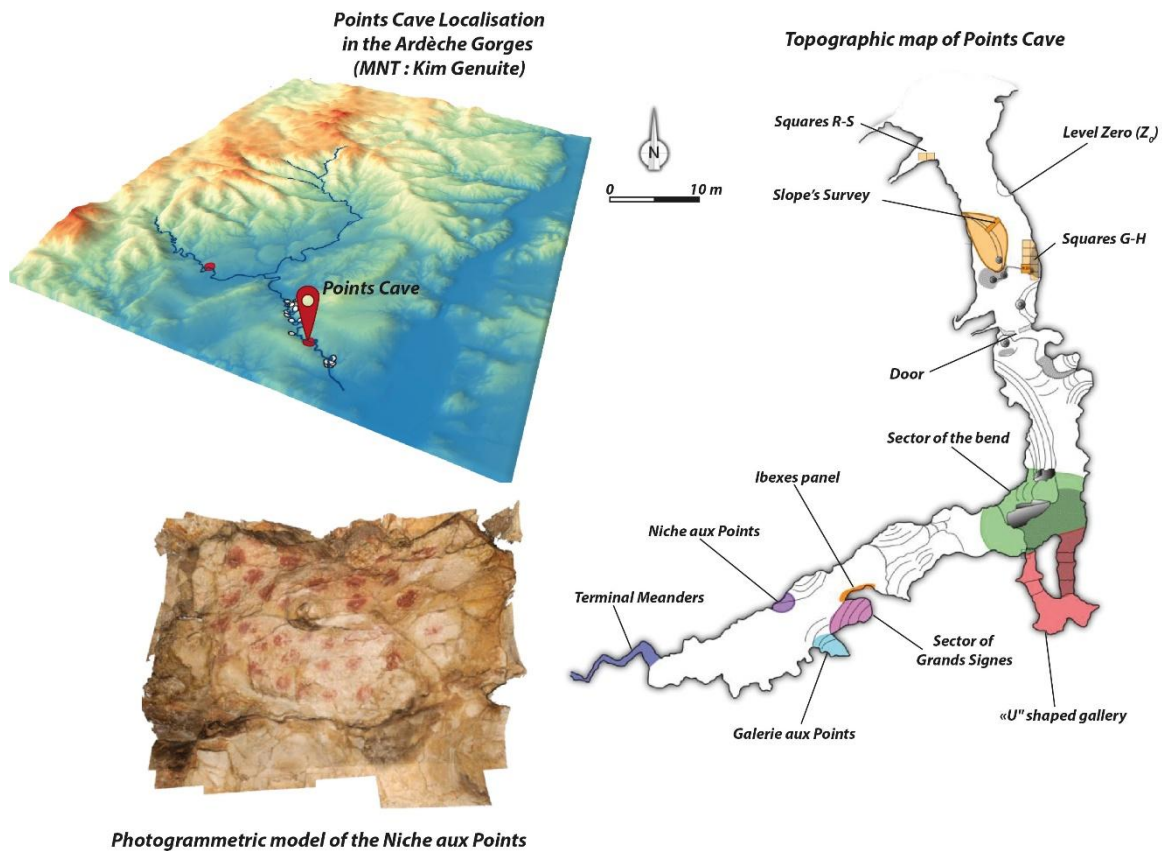
104 **2. Material**

105

106 **2.1 Study site: Points Cave**

107

108 Located in the Ardèche River gorge less than 10 km downstream of Chauvet Cave, Points Cave is a
109 Palaeolithic rock art site identified in 1993 (Figure 1) (Deschamps *et al.*, 2018). Archaeological studies
110 have been performed since 2011 as part of the “Datation Grotte Ornées” project (“Cave Art Dating”
111 project, Monney, 2011; 2018). The entrance opens on a hundred-metre long gallery in Urgonian
112 limestone. Rock art, exclusively composed of red imprints, is present in a unique sector in the middle
113 part of the gallery, preserved from sunlight. Excavations conducted at the entrance indicated human
114 and animal occupation during the Upper Palaeolithic (Monney & Jaillet, 2019).



116

117

118

Figure 1: Points Cave location in southeastern France and topographic map; photography of graphic entities: "Niche aux Points".

119

120 Points Cave is currently disconnected from hydrogeological flows (Jaillet & Monney, 2018). Only a
 121 few infiltrations can be observed after strong precipitation events. The low level of leaching on the
 122 wall and the quasi-absence of a calcite veil are due to this weak hydrogeological activity. Millimetric
 123 to centimetric concretions and efflorescences (coralloid type of crystallization) have developed on the
 124 wall surface in the decorated sector.

125

126 **2.2 Points Cave pictorial matter**

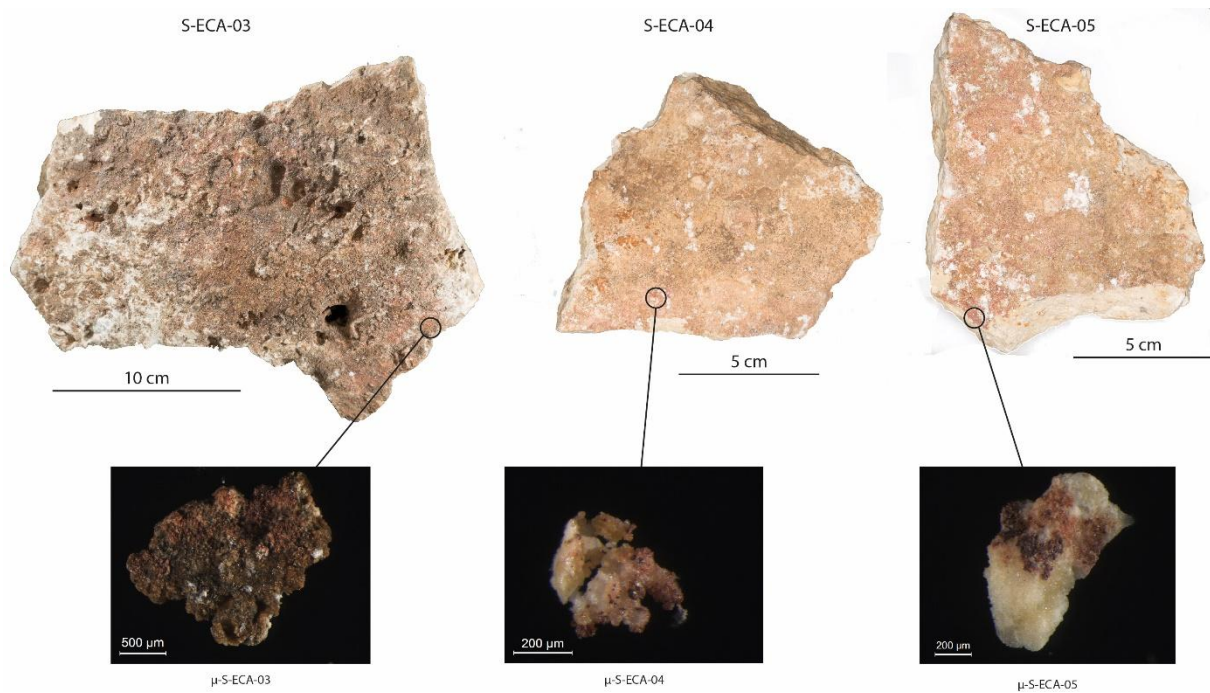
127

128 Parietal ornamentation, composed exclusively of reddish tracings and paintings, is currently observed
129 in the middle part of the gallery. It comprises 59 palm-printed dots, commonly referred to as "palm
130 points". This ornamentation also consists of five animal representations (three ibexes, a horse and a
131 bison), two bilobed signs, an angular line and a few indeterminate traces (isolated lines and dots)
132 (Monney, 2018). Moreover, archaeological colouring matter has been found in this sedimentary
133 sequence at the entrance of the cave (Chanteraud & al., 2019; Chanteraud, 2020).

134

135 Investigations carried out at the foot of the rock art panel known as the "Great Signs" found five
136 coloured wall flakes: S-ECA-01 to S-ECA-05 (Figure 2). Composed of limestone detached from the
137 wall under mechanical action, these 3 to 20 cm flakes are covered on one side with colouring matter,
138 probably coming from the large bilobed sign (graphic entity PTS-10) or from other unknown rock art
139 panels that may have crumbled entirely from the walls nearby. These flakes are a major asset of Points
140 Cave because they allowed us actual fragments of the decorated wall and transport them to the
141 laboratory.

142



143

144

145 **Figure 2:** Limestone flakes found at the foot of the Bilobed Signs panel, location of μ -sampling.

146

147 To identify both the iron-oxide morphologies and the natural mineralization that can form on the
 148 surface of the decorated walls, our study was centred around the five wall flakes discovered in the
 149 decorated sector of Points Cave and the 20 μ -samples taking from the decorated panels of the cave.
 150 One μ -sample of pictorial matter was performed on each coloured flake (μ S-ECA-01 to μ S-ECA-05).
 151 All μ -samples were observed and analysed without any preparation (Figure 2).

152

153 3. Methods

154

155 3.1 Macroscopic and microscopic observations

156

157 3.1.1 Laboratory and in situ observations at macroscopic scale

158

159 Image capture for macroscopic observations was performed in two steps: 1) a photograph was taken

160 under white light, and 2) another photograph was taken under UV light illumination. Observations at
 161 the macroscopic scale in the laboratory and in the cave were realized with a Canon EOS 5D Mark III
 162 camera and a Canon EOS 7D camera fixed on a tripod. A detached flash was used for image capture
 163 under white light. For UV light illumination, 4 UV LEDs (280 nm, 2.26 W, NewEnergy) were fixed
 164 on orientable macroflash bars on each side (2 LEDs per side) of the camera, allowing both
 165 macrophotography and general views of cave walls. Camera parameters are available in Table 1.
 166

Table 1: Camera parameters used for both white and UV light illumination during field and laboratory macroscopic observations.

| | | | <i>Aperture</i> | <i>Obturation speed (sec)</i> | <i>Iso</i> |
|-------------------|-------------|------------------|-----------------|-------------------------------|------------|
| Laboratory | White light | | F/7.1 | 1/320 | 1600 |
| | UV light | | F/7.1 | 10 | 1600 |
| Field | White light | <i>Macro</i> | F/11 | ½ | 320 |
| | | <i>Wall view</i> | F/11 | 1/60 | 100 |
| | UV light | <i>Macro</i> | F/4.5 | ½ | 320 |
| | | <i>Wall view</i> | F/11 | 15 | 320 |

167
 168 Laboratory observations were also performed using a stereomicroscope (LEICA M165 C) under white
 169 and UV light. The same 4 LEDs were used for UV illumination.

171 3.1.2 Laboratory observations at the microscopic scale

172
 173 At the microscopic scale, observations of μ -samples of flakes on carbon tape were realized with a
 174 field-emission scanning electronic microscope (SEM) ZEISS Ultra+ associated with an EDX (energy

175 dispersive X-ray) probe (SDD, Bruker) working in high-vacuum mode with a 15 keV voltage. Images
176 were taken with secondary electrons using in-lens or Everhart-Thornley detectors (SE2) and with
177 backscatter electrons (BSE-AsB detector) (Néel Institut, Grenoble).

178

179 **3.2 UV fluorescence analyses**

180

181 Stationary fluorescence signal of flake and flake μ -samples was measured in the laboratory with a
182 solid-phase spectrofluorimeter designed in the EDYTEM laboratory for non-destructive solid-phase
183 measurements (Perrette *et al.*, 2000).

184

185 This instrument is divided into excitation and detection compartments associated with a translation
186 stage system for sample surface measurement. For this experiment, the excitation system was
187 composed of a Nd:YAG laser (Crylas, FQSS266-Q1) with a 266 nm excitation wavelength. The
188 fluorescence emission response was collected after sample excitation by focusing the laser beam (~ 30
189 μm) on its surface. The detection system was composed of a low-pass filter monochromator (Jobin
190 Yvon, MicroHr) for light diffraction, fitted with a 300-g/mm diffraction-grating centred at 620 nm,
191 associated with a thermoelectric-cooled, back-illuminated CCD (Jobin Yvon, Sincerity) for high-
192 efficiency signal detection in the UV-visible light domain. As no manipulation, modification or
193 destruction of the sample surface occurred during analysis, this technique is suitable for archaeological
194 sample measurements.

195

196 Two types of fluorescence measurements were realized:

- 197 - Single point measurements were performed on flake μ -samples ($\mu\text{S-ECA-03}$, $\mu\text{S-ECA-04}$ and
198 $\mu\text{S-ECA-05}$). One spectrum was independently acquired on the sample. Measurement location
199 was determined manually. An acquisition time of 1 s and a monochromator entrance slit of
200 0.25 mm (~ 1 nm spectral resolution) were used for spot spectrum acquisition.
- 201 - Surface measurement was performed on flake S-ECA-05. The motorized translation stage

202 system allowed movements in two directions for surface measurements. The image was
203 obtained by stacking lines along the Y-axis. For this study, fluorescence surface imaging was
204 performed with a 100×100 µm resolution using a 0.1 s acquisition time and a 0.05 mm
205 entrance slit.

206

207 Data pre-processing was performed with MATLAB software. Spectra were corrected from baseline
208 and instrument responses and then filtered with the Savitsky-Golay method (Savitzky & Golay
209 1964).

210

211 **4. Results**

212

213 *4.1 Macroscopic scale observations*

214

215 At the macroscopic scale, no mineralization was observed on the walls, flakes or µ-sample surfaces.
216 Here, the coralloid type of crystallization was not taken into account due to its centimetric size. In fact,
217 at this observation scale, surfaces seemed to be well preserved with strong colouration from the
218 pictorial matter and clear access to the calcareous substrate (Figure 2).

219

220 It has been shown that decorated panels of the cave display various mineralizations, such as calcium
221 sulphate (Chanteraud *et al.*, 2020). However, these deposits remain invisible even after inspection
222 under a stereomicroscope, revealing the need for microscopic inspection using SEM.

223

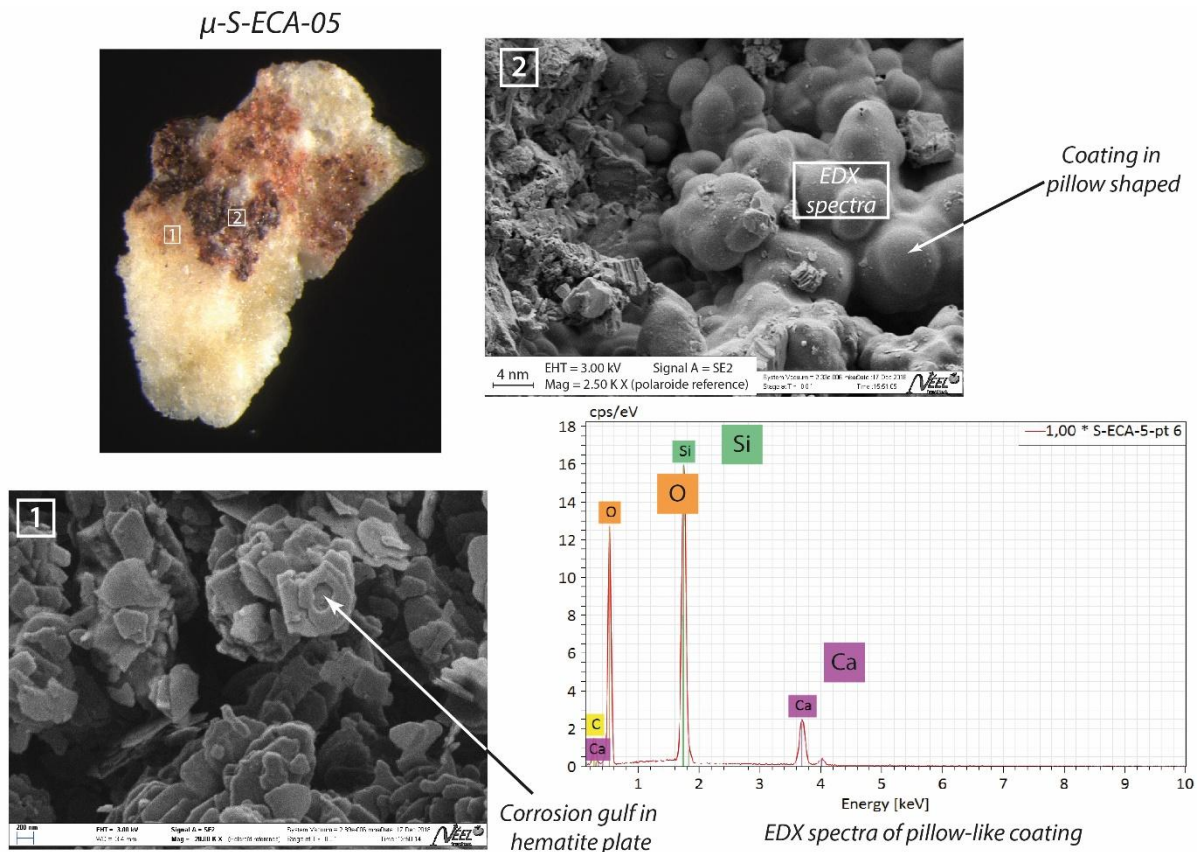
224 *4.2 Microscopic scale observations*

225

226 At the microscopic scale, a 1 µm-thin mineral film consisting of nonordered spheres was identified as
227 silica mineralization on flake µ-samples (Figure 3). Its geochemistry and hummocky morphology are

228 related to a type A-g amorphous opal with a $\text{SiO}_2 \cdot n\text{H}_2\text{O}$ formula (Flörke *et al.*, 1991). The mineral
 229 structure present on coloured flakes suggested its formation from a water film containing a high
 230 concentration of silica (Monger and Kelly, 2002; Curtis *et al.*, 2019).

231



232

233

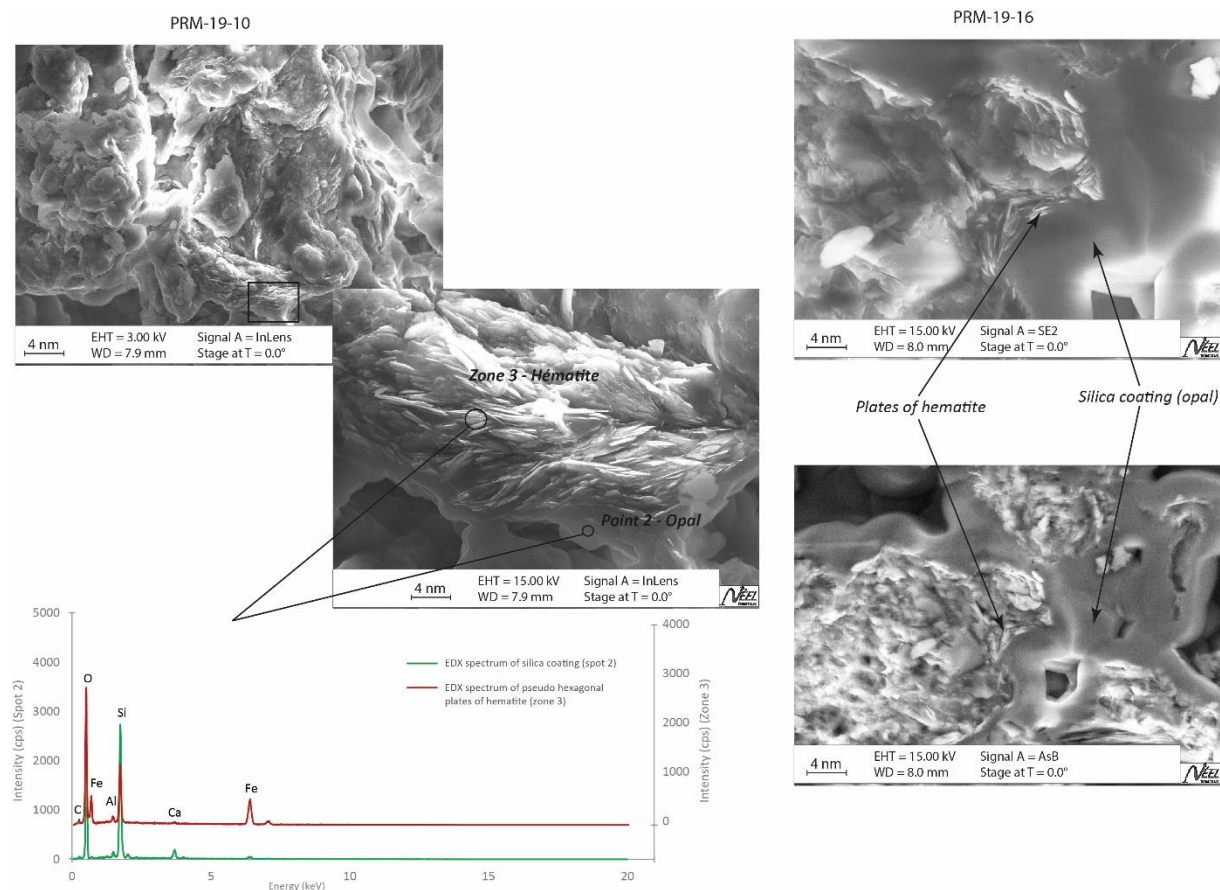
Figure 3: SEM observations of $\mu\text{-S-ECA-05}$. 1/ Corrosion gulf in hematite plate observation in Secondary Electron mode (SE); 2/ Pillow-like silica coating on surface in SE mode; White rectangle = Area of EDX spectra on the pillow-like silica coating.

234

235 Concerning the μ -samples from the decorated walls, the same observations were noted, including
 236 pseudo-hexagonal platy haematite and some strong indications of opal. Importantly, these samples
 237 showed significant opal development, with a complete coating of the pictorial matter to the extent that
 238 the morphology of the haematite was no longer observable on the surface.

239
240
241
242
243
244
245
246
247

SEM observations of flake μ -samples allowed us to identify pictorial matter as haematite due to its colour and macro- and micromorphologies. Typically, the haematite composing the pictorial matter was pseudo-hexagonal and showed corrosion gulfs (Figure 3). Weathered haematite plates seem to have been "ingested" by the silicate coating and could only be observed when a section was accessible on the surface of the sample (Figure 4). However, preliminary studies on the walls of Points Cave using portable spectroscopic techniques (pXRF and Raman) could not identify the presence of opal coating *in situ* (Chanteraud *et al.*, 2020).



248
249

Figure 4: Haematite plates embedded in the opal coating on PRM-19-10 and PRM-19-16 μ -samples (SEM observation in SE and BSE mode).

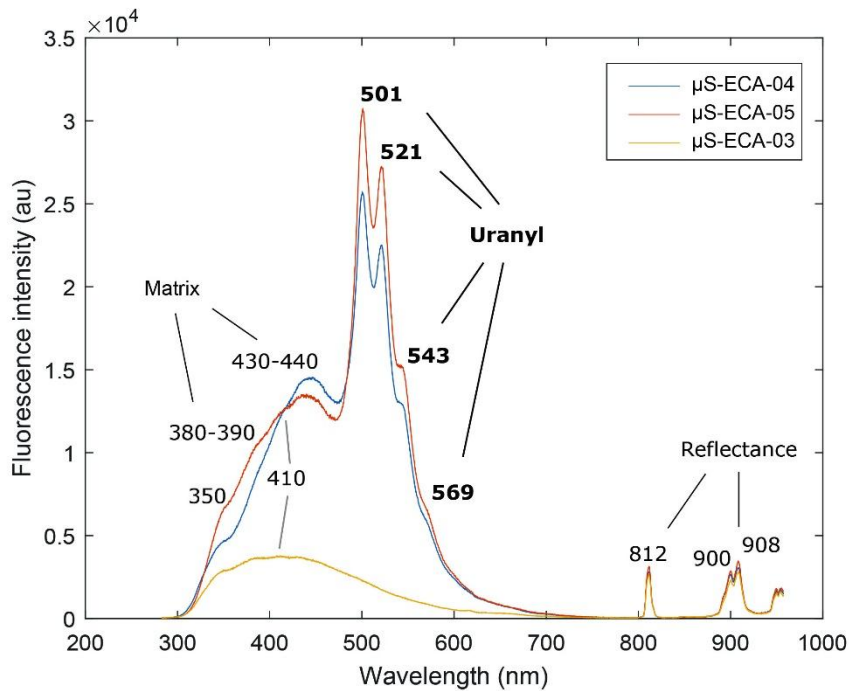
250

4.3 Opal identification by UV-fluorescence

251
252
253
254
255
256
257
258
259
260
261
262
263
264
265
266
267
268
269
270
271

To evaluate the potential of UV fluorescence to detect the opal mineral phase, fluorescence analyses were first performed on 3 flake μ -samples (μ S-ECA-03, μ S-ECA-04 and μ S-ECA-05) that were previously characterized by different geochemical analyses. Due to the small size of the samples (approximately 200 μ m), only a few localized spectra were recorded. The spectra obtained could be divided into different emission regions depending on the main signal sources (Figure 5):

- From 300 to 470 nm, this region corresponds to the fluorescence emission of the sample matrix. Peaks and shoulders were detected at approximately 350 nm, 380-390 nm, 410 nm and 430-440 nm. According to the literature, they could be associated with organic matter entrapped in the crystalline matrix (McGarry & Baker, 2000; Perrette *et al.*, 2000; Van Beynen *et al.*, 2001; Perrette *et al.*, 2005; Quiers *et al.*, 2015) or with the silica material fluorescence response to UV-light excitation (Boyko *et al.*, 2011; Garcia-Guinea *et al.*, 2013).
- From 470 to 750 nm, special features were identified in this part of the spectra for samples μ S-ECA-04 and μ S-ECA-05. They were characterized by a sequence of 3 defined peaks at 501, 521, and 545 nm and a shoulder at approximately 572 nm. These peaks were identical in all spectra measured on μ -samples μ S-ECA-04 and μ S-ECA-05 and coincided with the uranyl ion spectrum in silica matrices based on a review in the literature (Table 2).



272

273

274 **Figure 5:** Mean fluorescence emission spectra (excitation 266 nm) of samples μ S-ECA-04 (blue), μ S-
 275 ECA-05 (red) and μ S-ECA-03 (orange). Spectra are divided into three different regions as a function
 276 of the main fluorescence signal sources: sample matrix, uranyl ions and laser emission reflectance.

277

278 Entrapment of uranyl ions in siliceous matrices, especially opal phases, is well documented in the
 279 literature (Zielinski, 1980; Kasdan *et al.*, 1981; Kinnunen & Ikonen, 1991; Neymark *et al.*, 2000;
 280 Fritsch *et al.*, 2001; Gaillou *et al.*, 2008; Devès *et al.*, 2012; Fritsch *et al.*, 2015; Othmane *et al.*, 2016).
 281 The strong affinity of uranyl groups for amorphous silica leads to a strong U-opal association, which is
 282 stable at the scale of geological time (Othmane *et al.*, 2016). Thus, uranyl-specific spectra could be
 283 associated with the presence of opal on samples, and UV fluorescence analysis represents an efficient
 284 tool for its identification. As opal detection was subject to uranyl fluorescence properties, detection
 285 using UV fluorescence was dependent on uranium entrapment in silica crystalline structures. In their
 286 study of opal gems from different geographic and geological contexts, Gaillou *et al.* (2008) showed
 287 that not all opals are fluorescent. Opal fluorescence can be divided into two classes: blue fluorescence

288 caused by intrinsic oxygen-related defects typical of amorphous silica structures and green
 289 fluorescence attributed to uranyl groups (Fritsch *et al.*, 2001, 2003), which is believed to be typical of
 290 common opals. A low content of U (≥ 1 ppm) automatically induces a green fluorescence response to
 291 UV light excitation and can reach more than 100 ppm in some deposits (Gaillou *et al.*, 2008). Garcia-
 292 Guinea *et al.* (2013) measured a uranium amount of 193 ppm in stalactites in Castanar Cave. Thus,
 293 detection of opal via UV fluorescence is not systematic but common, as a low content of uranium
 294 allows fluorescence emission. However, uranium concentration in Points Cave μ -samples have not
 295 been measured due to the particularly thin opal layer and the impossibility of destroying μ -samples.

296

297 **Table 2:** Fluorescence emission peaks for different opal or amorphous silica deposits reviewed in the
 298 literature.

299

| | Fluorescence emission peaks (nm) | | | | |
|----------------------------------|---|------------|------------|------------|-----|
| | 504 | 524 | 546 | 570 | - |
| Othmane <i>et al.</i> 2016 | 504 | 524 | 546 | 570 | - |
| | 504 | 523 | 545 | 573 | - |
| Fritsch <i>et al.</i> 2015 | 504 | 524 | 546 | 572 | 604 |
| Brennan & White 2013 | 502 | 520 | - | - | - |
| Garcia-Guinea <i>et al.</i> 2013 | 505 | 524 | 543 | 569 | 650 |
| <i>This study</i> | 501 | 521 | 545 | 572 | - |

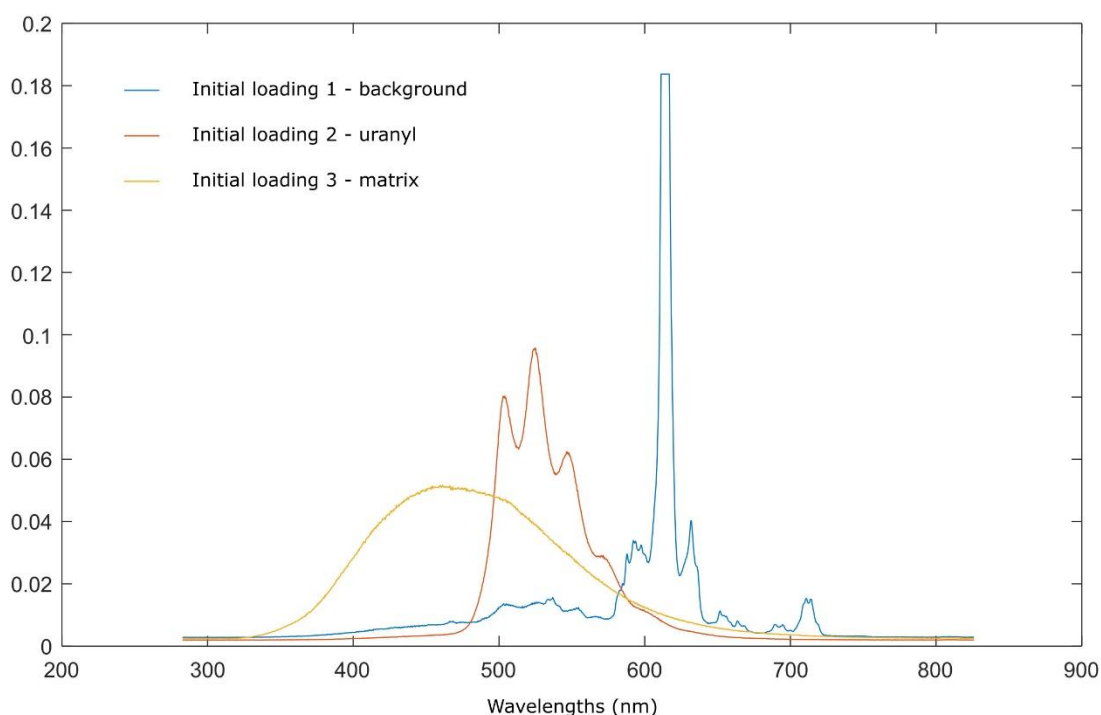
300

301

302 To evaluate method accuracy at a larger scale, a second experiment was performed directly on flake S-
 303 ECA-05. UV fluorescence cartography (100 x 100 μ m resolution) showed a range of spectra
 304 presenting uranyl spectral characteristics. Assuming that the fluorescence signal can be interpreted as a
 305 mixing of a uranyl signal with a matrix signal, opal information was extracted from fluorescence
 306 cartography using a mixing algorithm, MCR-ALS, with the MCR-ALS toolbox in MATLAB software

307 (Jaumot *et al.*, 2015). MCR-ALS has become a popular chemometric method in solving mixture
308 analytical models. It is based on an additive bilinear model of pure contributions that depends on the
309 concentration and the specific spectral sensitivity of each component. This algorithm can also be
310 applied to obtain quantitative information (Jaumot *et al.*, 2005; de Juan *et al.*, 2014; Zhang & Tauler,
311 2013). A singular value decomposition (SVD) method was first used in the MCR calculation to define
312 the number of initial loadings. Thus, three components were estimated that mainly contributed to the
313 fluorescence signal. These three initial loadings were calculated using the PURE algorithm, a
314 commonly used method to find the purest variable, and could be associated with uranyl fluorescence
315 spectra, matrix fluorescence signal and background signal (Figure 6).

316



317

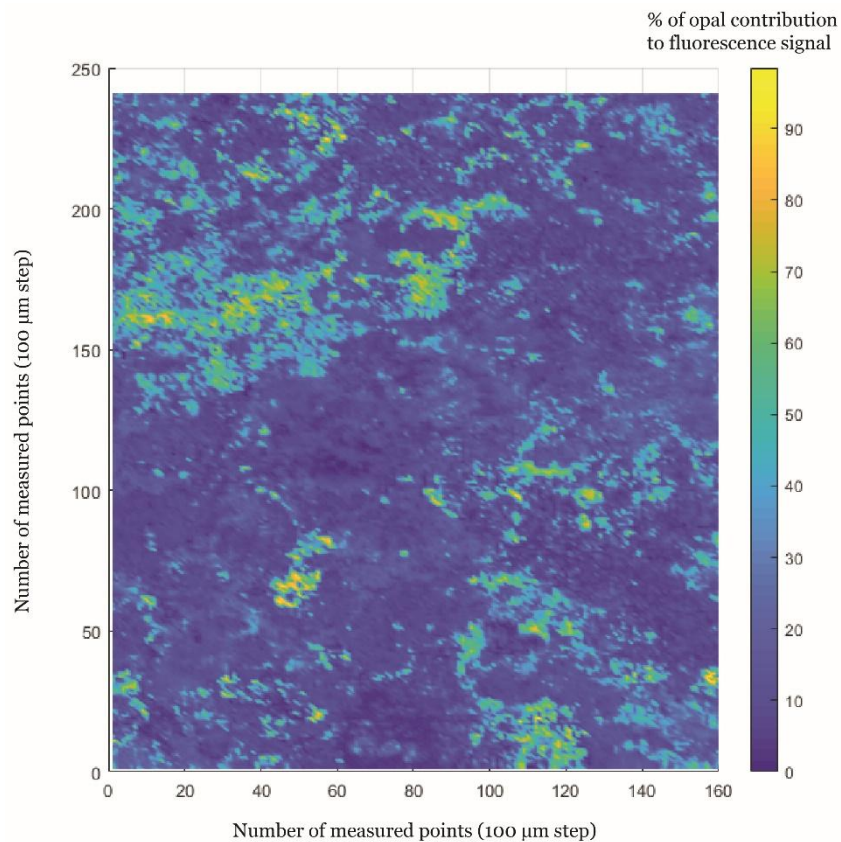
Figure 6: Initial loadings obtained with the PURE algorithm on fluorescence cartography spectra.

318

319 MCR-ALS was then performed based on these 3 initial loadings. Non-negativity constraints were
320 applied. Model results ($r^2=99.88$) indicated a contribution of uranyl to the sample fluorescence signal

321 and thus to a proportion of opal at the sample surface (Figure 7).

322



323

Figure 7: Opal fluorescence signal proportions measured on the S-ECA-05 flake and obtained with the MCR-ALS algorithm.

324

325 Evaluation of opal proportions on the sample using this method is, however, subject to certain biases.

326 Similar to the majority of spectroscopic techniques, this detection method can only detect surface
327 deposits. Thus, opal mineralization located under other mineral or organic deposits cannot be detected.

328 Moreover, for quantitative measurement, the measurement sensitivity to changes in sample surface
329 microtopography must be taken into account. As the laser beam is focused on the surface, variations in

330 fluorescence intensities measured on the sample, and thus opal estimations, can be biased by

331 millimetric changes in surface relief.

332

333 In addition, this method remains effective in extracting information on opal mineralization even on
334 heterogeneous matrices, such as the Points Cave μ -samples. Due to its specific spectral shape, uranyl
335 signal can be easily extracted from mixed fluorescence signals. In addition, mixing algorithms could
336 provide quantitative information if combined with calibration methods. Indeed, the MCR-ALS
337 algorithm has been used for the quantification of different target molecules based on various
338 spectroscopic data (Mas *et al.*, 2010; Araya *et al.*, 2017; Kumar *et al.*, 2018; Castro *et al.*, 2021).
339 Regarding sample complexity, calibration protocols based on standard references and prepared or
340 artificial mixtures are difficult to apply (Araya *et al.*, 2017). Quantification strategies need to be
341 developed for archaeological materials, reaching a balance between sample destruction and model
342 result robustness, such as those developed for hyperspectral data. Then, the estimated concentration
343 accuracy will depend on the legitimacy of the assumption made in the quantification strategy (Araya *et*
344 *al.*, 2017).

345

346 *4.4 Visual detection under UV light: laboratory experiments*

347

348 As explained previously, minerals containing uranyl ions (UO_2^{2+}) have been known to exhibit strong
349 fluorescence marked by specific spectral features and temporal characteristics since at least early 1900
350 (deNeufville *et al.*, 1981). The bright green fluorescence of uraniferous opal is a well-known
351 characteristic of this mineral phase and has been related to the presence of uranium (Gorobets *et al.*,
352 1977; Fritsch *et al.*, 2001). To evaluate whether this specificity can be used for opal detection, flake μ -
353 samples were exposed to UV light (see 3.1.1). The results show that μ -samples μ S-ECA-04 and μ S-
354 ECA-05 exhibited a bright green-light response (Figure 8). These two sample spectra contained
355 specific features corresponding to the fluorescence emission of uranyl ions. Green illumination was
356 thus associated with the presence of U-opal on these samples. The case of μ -sample μ S-ECA-03 was
357 more complex. While the fluorescence spectrum did not show any spectral features associated with the
358 uranyl signal, localized greenish fluorescence could be distinguished on the sample. This could be

359 explained by a less precise measurement due to a more difficult targeting of opal because of the higher
360 sample size or more scattered opal distribution. Second, the sample surface was more coloured and
361 had more pictorial matter (cf. §4.1), suggesting decreased ability for detection.

362

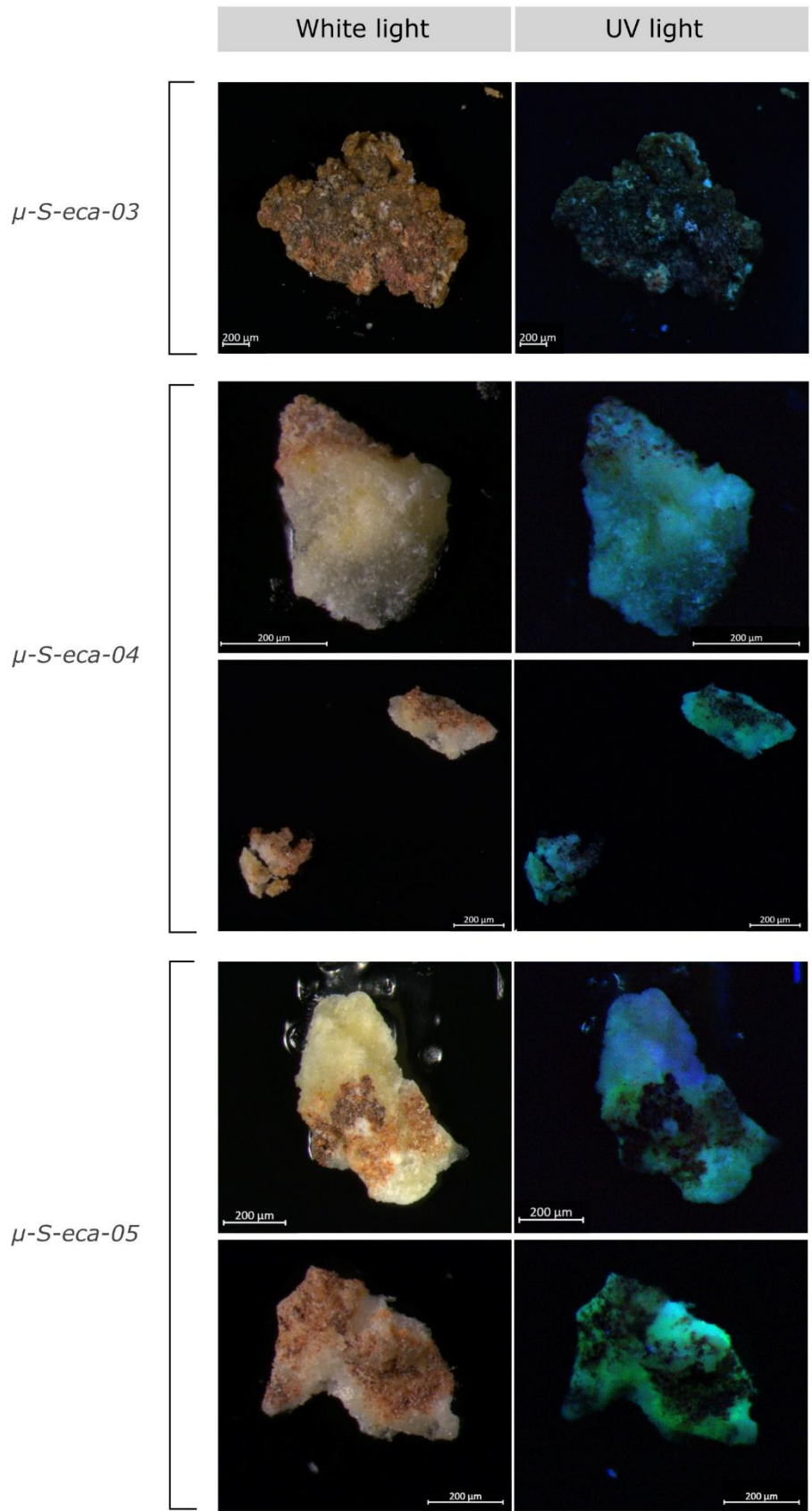


Figure 8: Photographs of three μ -samples taken on flakes under white and UV light.

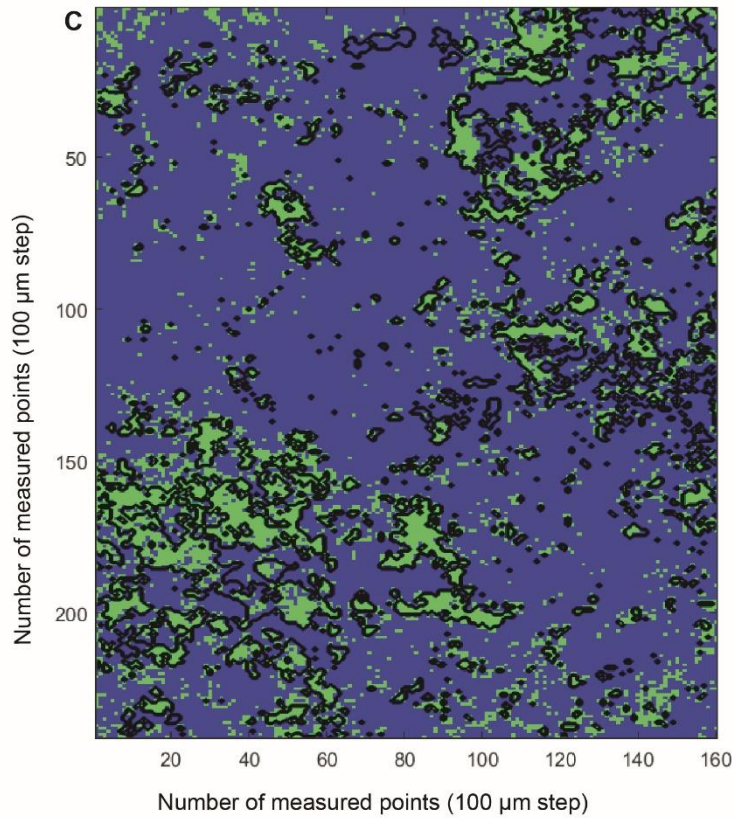
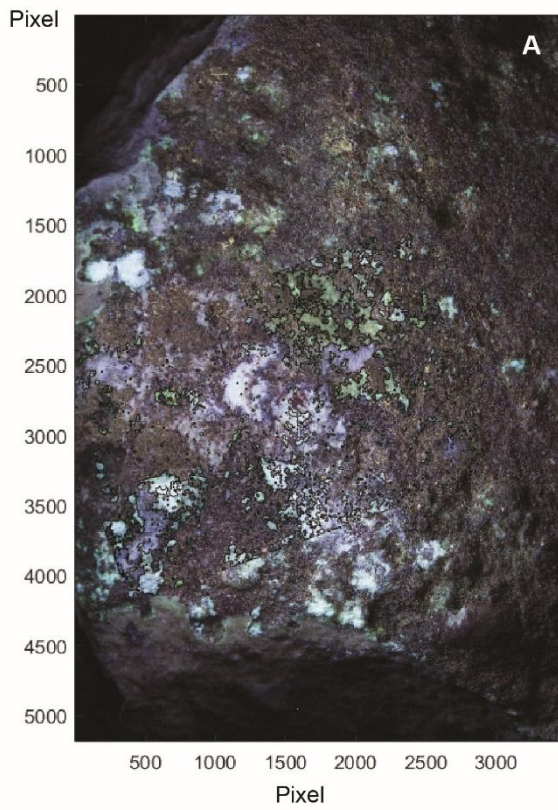
364

365 Considering that uranyl green illumination is representative of the presence of opal, detection
366 concordance between spectral and visual techniques was tested at a larger scale by comparing UV-
367 illuminated photographs with UV fluorescence cartography of flake S-ECA-05 (Figure 9). For this
368 purpose, the green component of the RGB image was extracted from UV-light photos. The grayscale
369 image was subtracted to avoid the luminosity effect, and a threshold was applied to the image obtained
370 to select only pixels containing green colour. To help compare the opal information provided by both
371 techniques, images were aligned using point control selection and geometric transformation functions
372 in MATLAB.

373

374 The results show a high correspondence between spectral and visual detection methods. To evaluate
375 the efficiency of the optical method, opal cartographies with different detection limits were simulated
376 using the opal contribution percentage to the fluorescence signal from spectroscopic measurements
377 and compared with optical data. The opal contribution threshold of 27% presented the best correlation
378 coefficient with opal extracted from UV photographs ($R^2=0.50$). This indicated that opal detection
379 with the optical method was efficient when opal fluorescence emission contributed at least 27% of the
380 total fluorescence signal of the sample. Under this threshold, the detection efficiency decreased for the
381 optical method. The rather low correlation coefficient between both images could mainly be explained
382 by the point control selection and geometric transformation applied to readjust them together. Angle
383 disposition of the sample and detector combined with image resolution could have led to difficulties in
384 adjusting the images. Further research in the computational image domain could improve the
385 methodology and enhance the correlation between the two techniques.

386



A - Photo under UV light with contour plot (black line) of opal location obtained by extraction of the green component of the image

B - Photo under UV light with contour plot (black line) of opal location obtained by MCR-ALS on fluorescence map

C - Opal location on sample obtained from fluorescence signal (green zones, 27% of signal contribution) and from UV photo (black lines)

387

388

Figure 9: Detection and location of opal mineralization on flake S-ECA-05 obtained using UV illumination (A) and UV fluorescence techniques (B).

The two methods are compared in C.

389

390

4.5 Visual detection under UV light: field experiments

391

392 An *in situ* photographic protocol that alternated white light and UV illumination was applied to the
393 Points Cave walls. As shown in Figure 1, three rock art panels were investigated with one wall where
394 rock art was absent. Images were realized at both the wall and macroscopic scales.

395

396 At the wall scale, the rock art panels investigated (Niche aux Points, Bilobed Signs and Ibexes)
397 displayed large green fluorescent zones when illuminated by UV LEDs (Figure 10). This green
398 fluorescence response was consistent with preliminary results obtained in the laboratory on cave wall
399 flakes and μ -samples from these zones. Thus, UV illumination successfully enabled the detection of
400 opal coatings on these walls, according to the green response observed in photographs.

401

402 In contrast, no opal signal appeared clearly distinguishable in photographs of the wall situated a few
403 metres before the art panel. These photographs displayed greenish fluorescence mixed with other
404 signals, making it difficult to identify and extract green colour with accuracy. Spectroscopic
405 measurements need to be performed to precisely identify the presence of opal.

406

407 Macroscopic-scale observations under UV light allowed the targeting of specific deposits or zones on
408 cave walls. In the particular case of the Bilobed Signs panel, macroscopic investigation targeting
409 flaking zones revealed a contrast between the rock art panel and the zones where flakes had detached
410 from the wall. Indeed, the left part of the UV photograph (Figure 10) displayed numerous green
411 fluorescent spots, whereas they were absent from the right part of the photograph. Efflorescence

412 concretions on cave walls, which are widely spread in Points Cave, were also investigated, but the
413 presence of opal has not yet been validated.

414

415 **5. Discussion: Implications of opal detection for rock art studies at Points Cave**

416

417 5.1 Contribution of UV fluorescence techniques

418

419 According to the first results obtained using the *in situ* UV illumination method and the preliminary
420 results obtained in the laboratory on cave wall flakes and μ -samples from rock art panels, *in situ*
421 measurements successfully detected the presence of opal in Points cave. Indeed, the green
422 fluorescence observed on Niche aux Points, Bilobed Signs and Ibexes panels suggests that opal
423 development covers a large area of cave walls, especially in rock art zones. Macroscopic observations
424 also help to provide initial insights into rock art-opal interactions, as UV light allows for the targeting
425 of specific deposits or zones on cave walls. It provides complementary information on opal
426 distribution and interaction with archaeological material. For example, investigation of the flaking
427 zone suggests a current absence of extended opal film or opal mineralization, probably due to
428 desquamation occurring on this wall.

429

430 However, the opal signal is not always clearly distinguishable, as observed on the wall outside of the
431 rock art zone or on coralloid concretions. Yet, these speleothems are known to contain a silica layer
432 enriched with uranium (Monney *et al.*, 2019; Barbarand et Nouet, 2020). Alternating layers of silica
433 and calcite or the presence of calcite cover could explain the ambiguous signal. First, this highlights
434 the need for *in situ* fluorescence spectroscopic measurements to validate the photographic
435 identification of the opal mineral phase in cases where the green response is not clearly detectable.
436 Second, colour perception varies greatly from one image to another, even within the same site, making
437 it difficult to evaluate the mineral phase distribution. Even if camera and image treatment parameters

438 influencing colour display (white balance, exposure time, filters, etc.) can be easily standardized,
439 lighting variations (LED orientation, position, distance from wall, etc.) are difficult to homogenize. As
440 this paper presents preliminary results attempting to validate the detection method, no protocol for
441 colour calibration was applied. Further research on the Points Cave site will be subject to the
442 development of a colour calibration procedure.

443
444 Finally, UV illumination also highlights various types of deposits, sometimes not clearly detected
445 under white light. After fluorescence analyses in the laboratory or directly *in situ*, this technique could
446 help to detect other mineral or organic phases. Moreover, it is interesting to note that UV illumination
447 emphasizes the presence of pigments due to their iron composition. Indeed, iron ions are known to
448 have a quenching effect on the fluorescence signal, including that of uranyl ions (Gaillou *et al.*, 2008;
449 Chen *et al.*, 2011). Thus, pigments appear clearly as no fluorescence zones on UV photographs, which
450 can be an interesting tool for rock art analysis, such as determination of sampling protocol or
451 dermatoglyph analysis.

452
453 Thus, UV methodology appears to be an efficient non-invasive tool for the *in situ* identification of U-
454 opal mineralization. Due to the green fluorescence resulting from UV excitation, it allows rapid *in situ*
455 detection of the opal mineral phase with direct results and very simple and low-cost equipment. As
456 this method has already been applied with success in some caves, rarely calcareous, for the detection
457 of U-silica complex deposits or concretions, as in Castañar Cave (Garcia-Guinea *et al.*, 2013), this
458 study differs in two ways. First, to our knowledge, this method has never been applied to opal
459 detection in a rock art context. Second, we propose *in situ* opal identification based on spectral
460 features for result validation using a portable UV-LIF instrument. This instrument is currently in
461 development and could not yet be taken into the cave, but preliminary tests applied to flakes in the
462 laboratory confirm its ability to detect opal. Finally, opal mineral characterization can also be achieved
463 with high-spatial resolution at the microscopic scale with a laboratory LIF instrument. Spatially high-
464 resolution fluorescence maps can also provide more information on mineral phase repartition,

465 development and interaction with other organic and mineral phases present on the sample. Thus, the
466 combination of these two methodologies provides a complete solution for the identification and
467 detection of opal mineralization in both sampling and analytical strategies and *in situ* characterization.

468

469 5.2 What do we know about Points Cave opal

470

471 The results obtained with the analyses presented in this paper and with UV methods applied to
472 samples and *in situ* have provided the first information on opal coatings in Points Cave. Indeed, based
473 on SEM analyses of flakes and μ -samples, Points Cave opal is associated with the amorphous opal
474 type (type A). XRD is usually performed for precise opal type determination (Curtis *et al.*, 2019).
475 However, in the case of Points Cave opal, this analysis is difficult to perform due to the opal thin layer
476 on calcareous substrate and iron-rich pigments. Analyses at macro- and microscopic scales suggest
477 thin film deposition as a mineralization type, such as silica skins observed at various rock art sites
478 (Watchman, 1990; Green *et al.*, 2017). This film appears to be deposited under or at the interface with
479 pigment and other crusts. SEM analyses show that the opal structure encapsulates haematite plates on
480 several samples, suggesting strong interactions with pictorial matter (Figure 4). Further studies must
481 be conducted to understand how these two phases interact, but a preliminary hypothesis regarding
482 dissolution and corrosion of haematite plaques by opal can be proposed.

483

484 The presence of uranyl ions entrapped in the opal structure was verified by UV spectroscopic analyses.
485 High fluorescence intensities of opal at Points Cave suggest significant content of uranium trapped in
486 the crystalline structure. Similar enrichment in uranium has been found in numerous common opals
487 (Amelin & Black, 2006). However, no quantification of uranium content has yet been realized.
488 Although uranium isotopic measurements were realized on speleothems from Points Cave (stalagmites
489 and coralloids), none was applied on flakes, or flake and wall μ -samples because of their destructive
490 character. According to the literature, as no minerals containing U⁴⁺ are known to fluoresce,
491 uraniferous silica precipitation involves oxidizing conditions sufficient to mobilize U⁶⁺ (Zielinski,

492 1982). For example, Garcia-Guinea *et al.* (2013) explained uranium-bearing opal deposition in
493 Castañar Cave by oxidation of host rocks with meteoritic waters. Zielinski (1982) explained that the
494 initial precipitation of silica was as an amorphous silica gel, with which dissolved uranium
495 coprecipitated before the silica gel dehydrated to form opal. The formation of uranyl-silica complexes
496 is favoured by the natural affinity between aqueous uranyl ions and the silica gel surface, which is
497 very sensitive to pH (optimum range = pH 5-5.5) (Garcia-Guinea *et al.*, 2013).

498

499 The *in situ* approach shows an important spread of this coating on Points Cave walls, especially on
500 rock art panels. Concerning the walls a few metres before the rock art panels, the presence of opal
501 needs to be confirmed by spectroscopic measurement and laboratory analyses. Points Cave chronology
502 is constrained by different periods marked by cave wall evolution under climatic and anthropogenic
503 factors (Monney & Jaillet, 2019). The presence of opal mineralization throughout its formation and
504 developmental processes could provide insights into cave chronology. A flaking period was identified
505 subsequent to ornamentation, resulting from mechanical expansion or desquamation, affecting the
506 deepest zones of the cave, and possibly concurrent with gelifraction during MIS2 (Marine Isotope
507 Stage 2) (Monney & Jaillet, 2019). As described previously, UV photographs indicated the absence of
508 a well-developed opal film in the flaking zone, suggesting that opal formation occurred principally
509 before this flaking period. This could also explain why photographs taken on walls between the cave
510 angle and the rock art sectors displayed less marked fluorescence, as this zone presents high flaking
511 rates (Jaillet & Monney, 2018) (Figure 12).

512

513 *Figure 10: Topographic section of Points Cave with estimated flaking and location of white*
514 *and UV light photographs according to Jaillet & Monney, 2018.*

515

516 The chronology of opal deposits over art paintings and drawings cannot be confirmed at this stage.
517 SEM observations show that opal mineralization colonizes empty spaces under, below, and inside
518 pictorial matter. These observations suggest opal postdeposition over painting realization, although

519 prior mineralization cannot be ruled out.

520

521 Thus, ongoing studies are crucial in completing opal coating characterization in Points Cave. This is a
522 tool in understanding cave wall and pigment interactions throughout the factors and processes of opal
523 formation and other mineralization.

524

525 *5.3 Opal factors and formation*

526

527 Mineralization origin and formation mechanisms and factors are clues for understanding past climate
528 and cave wall evolution. As this paper presents preliminary results, only hypotheses for opal origin
529 and formation are presented.

530

531 Opal, as a hydrated mineral, is associated with fluid circulation. Thus, water is generally involved in
532 precipitation, and silica has to be in solution before precipitation (Chauviré *et al.*, 2017). In Points
533 Cave, the presence of silica coating with high uranium content in the limestone context supports the
534 hypothesis of mineralization originating from groundwater. Wall humidification and water
535 physicochemical properties directly influence the coating formation rate. In very wet sites, the silica
536 skin growth rate can reach 0.25 mm per millennia, whereas occasionally wet sites present a
537 mineralization rate on the order of 0.02 mm per millennia (Aubert *et al.*, 2004). Silica coatings can
538 only be formed and preserved if low infiltration volumes occur, as higher volumes favour dissolution
539 of soluble compounds and decrease silica precipitation (Aubert *et al.*, 2004).

540

541 Chauviré *et al.* (2017) explained that even though opal is found in various geological contexts, three
542 main types of formation can be identified: 1) hydrothermal activity, 2) continental weathering and 3)
543 biological precipitation. As no hydrothermal activity was identified at Points Cave, only the latter two
544 types can be involved in opal formation at this site.

545

546 Biological formation of opal in caves is less documented than hydrothermal alteration and continental
547 weathering. Various microbial forms and algae have been observed to be associated with opal in
548 caves, such as siliceous algal diatoms (Northup *et al.*, 2001), and are often linked to coralloid
549 concretions. In the case of Points Cave, a few microscopic and cave wall μ -sample observations show
550 undetermined structures containing high carbon content, which could be associated with biological
551 activity. Nevertheless, the hypothesis of biological formation of opal cannot be ruled out or confirmed
552 at this stage, and further studies need to be conducted.

553

554 Continental weathering is defined by rock transformation by meteoric water and a precipitation
555 temperature below 50°C, in contrast to hydrothermal alteration (Chauviré *et al.*, 2017). Silica anions
556 released by this process precipitate because of fluid supersaturation due to various changes in
557 conditions, such as pH or temperature (Devès *et al.*, 2012; Chauviré *et al.*, 2017). Thus,
558 supersaturation of silica solutions may be initiated by a drop in temperature or pH or an increase in
559 salinity. When a solution is supersaturated in SiO₂, silicic acid could polymerize to form a colloidal
560 suspension from which amorphous silica can precipitate. Polymerization is controlled by temperature
561 (decreasing T° increases the polymerization rate), degree of supersaturation, salinity and mainly pH
562 (maximum polymerization rate around pH 7.5; minimum polymerization rate under pH 3 and above 9)
563 (Devès *et al.*, 2012). One of the most efficient pH-driven mechanisms for silica precipitation involves
564 acidification of highly alkaline solutions (Zielinski, 1982). Such alkaline conditions are not common,
565 but in the case of calcite-dominant material in sediment, pH could reach this threshold (Karkanis *et al.*,
566 1999). Freezing temperature has also been shown to help supersaturation, polymerization and
567 rapid precipitation of opal, whereas low or moderate temperatures induce slow polymerization
568 (months or years) (Devès *et al.*, 2012). Cryo-segregation is another reported genesis, caused by
569 moisture freezing on cave walls, which concentrates dissolved salts. They precipitate out in the case of
570 supersaturation of the solution (Devès *et al.*, 2012). As opal formation probably occurred between the
571 Upper Palaeolithic and the Last Glacial Maximum and because freezing temperatures have been
572 shown to have modified Points Cave wall topography, a temperature decrease represents a realistic

573 factor for opal formation. However, there is currently a lack of evidence to confirm this hypothesis.

574

575 Silica solutions can originate from 1) superficial cover, 2) host rock, or 3) volcanic ash in a continental
576 weathering context (Devès *et al.*, 2012). Volcanic ash is an interesting hypothesis, as it is assumed to
577 provide high contents of silica and uranium and because the Ardèche region had recent volcanic
578 episodes during the Upper Palaeolithic. Indeed, Nomade *et al.* (2016) dated volcanic eruptions in the
579 Bas-Vivarais region between 29 ± 10 ka and 35 ± 8 ka and suggested that Chauvet rock art, 35 km
580 away, could depict volcanic eruption representations. The current alluvial plain and the lowest former
581 alluvial level (+8 m) deposits contain much basaltic material partly derived from Bas-Vivarais lava,
582 which were subjected to intense erosion and weathering in the alluvium terraces (Genuite *et al.*, 2021).
583 Thus, the location and chronology of the volcanic activity (approximately 45 km from Points Cave)
584 represent an interesting origin hypothesis for both silica and uranium contents in opal. However,
585 determining the origin of uranyl-enriched silica solutions is difficult with our current information.
586 Another hypothesis for silica solution origin can be supported by the presence of a marl layer within
587 the Urgonian limestone, which constitutes the cave environment (Sadier, 2013); or by pebbles
588 originating from the Ardèche River and providing silica by infiltration from the overlaying alluvium
589 terrace or by river deposition (Mocochain *et al.*, 2009; Genuite *et al.*, 2021).

590

591 Thus, understanding the origin and mineralization factors that influence opal formation could provide
592 information on chemical and physical processes occurring on the cave wall surface. According to
593 Green *et al.* (2017), this knowledge is “crucial for targeted sample collection and the application of a
594 range of dating techniques as well as for the development of conservation strategies”. Further studies
595 still need to be performed to identify opal origin and formation factors at Points Cave.

596

597 *5.4 Chronology and dating*

598

599 Red pigments used in rock art are difficult to date precisely (Aubert *et al.*, 2007). Thus, several studies

600 have proposed indirect dating methods using associated mineral deposits interlaying pictorial matter to
601 date or to provide chronological constraints on rock paintings (Watchman, 1990; Aubert *et al.*, 2007;
602 Aubert *et al.*, 2017), such as opal coatings.

603
604 Indeed, in the first place, opal coating could help to precise relative chronology thanks to knowledge
605 regarding climatic and environmental factors controlling its mineralization, and to its distribution on
606 walls in comparison to other deposits and archaeological material.

607
608 Amorphous silica skins have been used for radiocarbon analyses based on organic remains trapped by
609 mineralization, such as diatoms or algal matter, on different Australian rock art sites (Watchman,
610 2000; Morwood *et al.*, 2010). However, as silica coatings may contain various organic materials, each
611 presenting a specific radiocarbon signature, dating could result in a mixture of different ages by
612 incorporation of younger or older material (Aubert *et al.*, 2017; Green *et al.*, 2017). In addition, the
613 formation processes of these coatings are not fully understood, requiring great caution when using
614 radiocarbon methods (Aubert *et al.*, 2017). Using compound-specific carbon analyses could
615 potentially avoid this problem (Aubert *et al.*, 2017) but are more difficult to apply to thin deposits,
616 especially in rock art contexts.

617
618 Moreover, opal often contains high uranium contents, which could be used for high-precision dating
619 with methods such as $^{230}\text{U}/\text{Th}$ or U/Pb (Zielinski, 1980; Oster *et al.*, 2017). Because of opal's ability to
620 concentrate uranium from water while rejecting Pb and Th, amorphous silica is an interesting
621 alternative to carbonate minerals (Amelin & Black, 2006). Indeed, $^{230}\text{Th}/\text{U}$ and U/Pb methods have
622 been applied to opal and have provided reliable ages (Neymark & Paces, 2013). They enable
623 chronological constraints or dating hydrogenic subsurface water flow, pedogenesis, and processes
624 such as ore formation deposits (Neymark & Paces, 2013). They also have been applied in the case of
625 paleoclimate reconstruction in silica speleothem studies (Lundberg *et al.*, 2010). Depending on the
626 formation processes, opal coating could thus be used for dating purposes.

627

628 In rock art research, dating of amorphous silica deposits could be used as an age constraint for rock
629 drawing events, depending on the pigments and mineral phase superposition. In their study, Aubert *et*
630 *al.* (2007) performed U-series dating on a 2.5 mm thick calcite coating using the MC-ICPMS
631 technique, allowing high spatial and temporal resolution. Even though only micrograms of samples are
632 needed, authors (Aubert *et al.*, 2007; Aubert *et al.*, 2017) have suggested that for samples with U
633 concentrations > 1 ppm, sampling could be largely reduced, and LIBS techniques could also be
634 applied *in situ* with a 100-200 µm diameter ablation spot. As opal concentrates more U than calcite,
635 these techniques appear to be possible. However, for some authors, the application of uranium series
636 dating to silica skins appears difficult to achieve (Green *et al.*, 2017). Sampling that provides sufficient
637 intact fragments for LA-ICP-MS analysis without damaging rock paintings is one of the main issues
638 regarding this application. The difficulty of performing closed system conditions and replicability tests
639 for evaluating dating reliability has also been highlighted by authors.

640

641 Moreover, methods for opal detection could offer supplemental help before sampling for dating.
642 Indeed, precise targeting of uranium-bearing opal enables identification of pure silica phases in mixed
643 samples, detection of high uranium contents or impurity avoidance. In the case of thin layer deposits,
644 such as coralloids, sampling could decrease dating accuracy when mixing different layers (Devès *et*
645 *al.*, 2012). Tracking the location of opal phases could avoid this issue by spatially constraining
646 sampling.

647

648 *5.5 Implication of opal mineral characterization for conservation of rock art material*

649

650 Taphonomy represents a range of transformations affecting archaeological material that distort
651 archaeological records. Thus, rock paintings have undergone a plurality of transformations impacting
652 pigment longevity, colour (Bednarik, 1994) and identification. The exceptional of Points Cave
653 dermatoglyphs has no comparison with other associated parietal sites in Ardèche and begs the question

654 of opal impact on pigment conservation.

655

656 The association of silica skins composed of opal and pigments has been frequently observed at rock art
657 sites, mainly in open-air sites on sandstone and quartzite substrates in Australia or Canada (Watchman,
658 1990; Aubert *et al.*, 2004; Aubert *et al.*, 2012; Huntley, 2012). Some studies have suggested that
659 pigment binding in silica coatings aids rock art visual preservation (Watchman, 1990), providing a
660 resistant layer to chemical weathering. SEM observations on Points Cave flake and wall μ -samples
661 indeed suggest a strong interaction between pigments and opal, as mineralization penetrates pigment
662 deposits. If the quality of Points Cave paintings tends to corroborate this hypothesis, exfoliation
663 impacting silica skins observed at some sites should also be mentioned, as it could cause removal of
664 associated pigments (Aubert *et al.*, 2004; Green *et al.*, 2017). Thus, exploiting the observed benefits of
665 silica film deposits for conservation strategies has not yet been proven (Green *et al.*, 2017).
666 Furthermore, it has also been observed at open-air sites that silica skins could reduce the colour tone of
667 paintings and drawings at some locations (Green *et al.*, 2017).

668

669 If pigment weathering can be influenced by their own properties by inducing changes in surface area,
670 albedo, light transmissivity or moisture (Huntley, 2012), mineral deposits have been recognized to be
671 important factors in rock art taphonomy (Chalmin *et al.*, 2018). In addition to analytical impacts,
672 knowledge of mineral phases is essential because it informs us regarding the physical and chemical
673 impacts on pictorial matter and whether they favour conservation or degradation effects. Mineral
674 phase characterization is thus an important part of conservation strategies, and adapted identification
675 and analytical methods are needed.

676

677 **6. Conclusion**

678

679 The methodological development proposed in this paper was motivated by the identification of opal in

680 different contexts: *in situ*, in the laboratory, on centimetric objects and on μ -samples. The aim of this
681 identification is to question the possibility of accessing the specificities of the colouring matter applied
682 on the walls (petrography and geochemistry). Therefore, *in situ* identification of silica coating
683 observed in the laboratory was crucial for further studies on pigment characterization.

684
685 The results obtained on flakes and flake μ -samples from Points Cave show that UV LIF is an efficient
686 technique to detect and identify uranyl-silica complexes, even on heterogeneous and complex surfaces.
687 Although opal coating detection is limited by scale (laser beam) and by the outcropping nature of the
688 deposit, UV LIF spectroscopy offers a rapid and non-invasive tool that can easily be brought to the site
689 and positioned in front of the decorated panels. A photograph of green bright fluorescence emitted by
690 opal was used here as a method of *in situ* detection of this mineral coating. A comparison with the UV
691 LIF method shows a great correspondence between the two methods. The first tests of UV
692 illumination in the cave highlight the need to develop an accurate measurement protocol, especially to
693 homogenize light and colour, and the need to validate the identification using UV spectroscopy. In
694 addition to further methodological development, UV optical technique shows great potential because it
695 successfully detects the presence of opal and its distribution on rock art panels.

696
697 Thus, the results obtained with our methodology provide insights into disturbances in the classical *in*
698 *situ* spectroscopic analyses (pXRF and Raman) observed at Points Cave. The identification and
699 characterization of opal coatings is thus essential because of their impact on *in situ* analysis, which
700 does not allow the detection of iron spectroscopic signal. For this reason, we propose early, on-site
701 observations combined with sampling of surrounding material, such as fallen flakes from cave walls,
702 as an alternative strategy to i) characterize pigment-associated mineral phases, ii) choose the best site-
703 adapted combination of techniques and devices for *in situ* analyses and iii) define laboratory analytical
704 strategies depending on the pictorial matter environment.

705 Moreover, optical methods with *in situ* visual detection, such as the UV light illumination method
706 proposed in this paper, represent an interesting tool to add to sampling and analytical strategies.

707 Visualization at a larger scale of the presence and distribution of mineral deposits that could interfere
708 with pigment analyses is a great help in locating sampling or *in situ* measurements to avoid
709 interference.

710

711 In addition to analytical impacts, the detection and identification of mineral phases can provide
712 valuable information on the pigment environment and human practice chronology. If speleothems are
713 considered an accurate archive for past climate and environment, other mineral deposits could provide
714 informative records on the setting and evolution of archaeological evidence. Applying a specific
715 methodology for their characterization is thus an efficient tool in improving rock art knowledge.

716

717 Thanks to opal mineralization detection utilizing UV methodologies on cave walls, a discussion on its
718 formation and associated factors, such as climatic, hydrologic or geomorphologic conditions over time
719 can be started. Thus, the mineral form described as opal-A can provide elements on cave natural
720 history.

721

722 **Acknowledgements**

723

724 We would like to thank Frédérique Charlot, microscopist at CMTC (INPE, Grenoble).
725 Funding was provided by ANR LabCom SpecSolE, DRAC Occitanie, DRAC AURA
726 (Pigmentoθήque project), French Ministry of Culture and University Savoie Mont Blanc.

727

728 **Conflict of interest disclosure**

729 The authors declare they have no conflict of interest relating to the content of this article.

730

731 **Data, script and code availability**

732 *SEM data:*

733 <https://doi.org/10.6084/m9.figshare.16832593.v2>
734 <https://doi.org/10.6084/m9.figshare.16832557.v3>
735 <https://doi.org/10.6084/m9.figshare.16832452>
736 <https://doi.org/10.6084/m9.figshare.16832605>
737 *Single UV fluorescence measurement (raw data):* <https://doi.org/10.6084/m9.figshare.16837180.v1>
738 *UV fluorescence cartography measurement (raw data):*
739 <https://doi.org/10.6084/m9.figshare.16837324.v1>
740 *UV fluorescence data processing (Matlab script):* <https://doi.org/10.6084/m9.figshare.16837405.v1>

741

742 **Bibliography**

743

744 Amelin, Y., Back, M., 2006. Opal as a U–Pb geochronometer: search for a standard. *Chemical*
745 *Geology* 232, 67–86.

746

747 Araya, J.A., Carneiro, R.L., Arévalo, C., Freer, J., Castillo, R. del P., 2017. Single pixel quantification
748 strategies using middle infrared hyperspectral imaging of lignocellulosic fibers and MCR-ALS
749 analysis. *Microchemical Journal* 134, 164–172.

750

751 Aubert, M., Brumm, A., Taçon, P.S., 2017. The timing and nature of human colonization of Southeast
752 Asia in the late Pleistocene: A rock art perspective. *Current Anthropology* 58, S553–S566.

753

754 Aubert, M., 2012. A review of rock art dating in the Kimberley, Western Australia. *Journal of*
755 *Archaeological Science* 39, 573–577.

756

757 Aubert, M., O’Connor, S., McCulloch, M., Mortimer, G., Watchman, A., Richer-LaFlèche, M., 2007.
758 Uranium-series dating rock art in East Timor. *Journal of Archaeological Science* 34, 991–996.

759

760 Aubert, M., Watchman, A., Arsenault, D., Gagnon, L., 2004. L'archéologie rupestre du Bouclier
761 canadien : Potentiel archéométrique. *Canadian Journal of Archaeology/Journal Canadien*
762 *d'Archéologie* 51–74.

763

764 Barbarand, J., Nouet, J., 2020. Pétrographie et minéralogie des coralloïdes de la grotte au Points, in:
765 Monney J. (Dir.). *Projet Datation Grottes Ornées : Rapport d'activité 2020. Grotte Aux Points*
766 (Aiguèze). Rapport Non Publié., Ministère de La Culture, SRA Occitanie, Montpellier.

767

768 Bassel, L., 2017. Genèse de faciès calcitiques : mondmilch et coralloïdes. Étude multiphysique des
769 concrétions de la grotte laboratoire de Leye (Dordogne) (Thèse). Université Bordeaux Montaigne.

770

771 Bednarik, R.G., 1994. A taphonomy of palaeoart. *Antiquity* 68, 68–74.

772

773 Boyko, V., Dovbeshko, G., Fesenko, O., Gorelik, V., Moiseyenko, V., Romanyuk, V., others, 2011.
774 New optical properties of synthetic opals infiltrated by DNA. *Molecular Crystals and Liquid Crystals*
775 535 (1), 30-41.

776

777 Castro, R.C., Ribeiro, D.S., Santos, J.L., Páscoa, R.N., 2021. Near infrared spectroscopy coupled to
778 MCR-ALS for the identification and quantification of saffron adulterants: Application to complex
779 mixtures. *Food Control* 123, 107776.

780

781 Chalmin, E., Hoerlé, S.H., Reiche, I., 2018. *Taphonomy on the Surface of the Rock Wall*. Oxford
782 University Press.

783

784 Chanteraud, C., 2020. *Matières colorantes et grottes ornées des gorges de l'Ardèche. Méthodes*
785 *d'analyse des ressources et liens culturels au Paléolithique supérieur : application à la grotte aux Points*

786 (Aiguèze, Gard, France) (Thèse). Université Savoie Mont Blanc.
787

788 Chanteraud, C., Chalmin, E., Hoerlé, S., Salomon, H., Monney, J., 2019. Relation entre les matières
789 colorantes issues des fouilles et des parois ornées. Méthodologie et première perspective comparative
790 à la Grotte aux Points (Aiguèze, Gard, France). *Karstologia* pp 1-12.
791

792 Chauviré, B., Rondeau, B., Mangold, N., 2017. Near infrared signature of opal and chalcedony as a
793 proxy for their structure and formation conditions. *European Journal of Mineralogy* 29, 409–421.
794

795 De Juan, A., Jaumot, J., Tauler, R., 2014. Multivariate Curve Resolution (MCR). Solving the mixture
796 analysis problem. *Analytical Methods* 6, 4964–4976.
797

798 Curtis, N.J., Gascooke, J.R., Johnston, M.R., Pring, A., 2019. A review of the classification of opal
799 with reference to recent new localities. *Minerals* 9, 299.
800

801 DeNeufville, J., Kasdan, A., Chimenti, R., 1981. Selective detection of uranium by laser-induced
802 fluorescence: a potential remote-sensing technique. 1: Optical characteristics of uranyl geologic
803 targets. *Applied Optics* 20, 1279–1296.
804

805 Deschamps, E.B., Chauvet, J.M., Hillaire, C., 2018. La grotte aux Points d’Aiguèze : récits de
806 découverte d’une ornementation pariétale. *Karstologia* 72, 13–14.
807

808 Devès, G., Perroux, A.-S., Bacquart, T., Plaisir, C., Rose, J., Jaillet, S., Ghaleb, B., Ortega, R., Maire,
809 R., 2012. Chemical element imaging for speleothem geochemistry: Application to a uranium-bearing
810 corallite with aragonite diagenesis to opal (Eastern Siberia, Russia). *Chemical Geology* 294, 190–202.
811

812 Flörke, O., Graetsch, H., Röller, K., Martin, B., Wirth, R., 1991. Nomenclature of micro-and non-

813 crystalline silica minerals. *Neues Jahrbuch für Mineralogie, Abhandlungen* 163, 19–42.

814

815 Fritsch, E., Megaw, P.K., Spano, T.L., Chauviré, B., Rondeau, B., Gray, M., Hainschwang, T., Renfro,
816 N., 2015. Green-luminescing hyalite opal from Zacatecas, Mexico. *J. Gemmol* 34, 490–508.

817

818 Fritsch, E., Mihut, L., Baibarac, M., Baltog, I., Ostrooumov, M., Lefrant, S., Wery, J., 2001.
819 Luminescence of oxidized porous silicon: Surface-induced emissions from disordered silica micro-to
820 nanotextures. *Journal of Applied Physics* 90, 4777–4782.

821

822 Fritsch, E., Wéry, J., Jonusauskas, G., Faulques, E., 2003. Transient photoluminescence from highly
823 disordered silica-rich natural phases with and without nanostructures. *Physics and chemistry of*
824 *minerals* 30, 393–400.

825

826 Gaillou, E., Delaunay, A., Rondeau, B., Bouhnik-le-Coz, M., Fritsch, E., Cornen, G., Monnier, C.,
827 2008. The geochemistry of gem opals as evidence of their origin. *Ore Geology Reviews* 34, 113–126.

828

829 Garcia-Guinea, J., Fernandez-Cortes, A., Alvarez-Gallego, M., García-Antón, E., Casas-Ruiz, M.,
830 Blázquez-Pérez, D., Teijón, O., Cuezva, S., Correcher, V., Sanchez-Moral, S., 2013. Leaching of
831 uranyl–silica complexes from the host metapelite rock favoring high radon activity of subsoil air: case
832 of Castañar cave (Spain). *Journal of Radioanalytical and Nuclear Chemistry* 298, 1567–1585.

833

834 Gorobets, B., Engoyan, S., Sidorenko, G., 1977. Investigation of uranium and uranium-containing
835 minerals by their luminescence spectra. *Soviet Atomic Energy* 42, 196–202.

836

837 Green, H., Gleadow, A., Finch, D., Hergt, J., Ouzman, S., 2017. Mineral deposition systems at rock art
838 sites, Kimberley, Northern Australia—Field observations. *Journal of Archaeological Science: Reports*
839 14, 340–352.

840

841 Huntley, J., 2012. Taphonomy or paint recipe: In situ portable x-ray fluorescence analysis of two
842 anthropomorphic motifs from the Woronora Plateau, New South Wales. *Australian Archaeology* 75,
843 78–94.

844

845 Huntley, J., Aubert, M., Ross, J., Brand, H. E., Morwood, M. J., 2015. One colour, (at least) two
846 minerals: a study of mulberry rock art pigment and a mulberry pigment ‘quarry’ from the Kimberley,
847 northern Australia. *Archaeometry* 57 (1), 77-99.

848

849 Jaillet, S., Monney, J., 2018. Analyse 3D des volumes et remplissages souterrains de la grotte aux
850 Points au temps des fréquentations paléolithiques (Aiguèze, Gard). *Karstologia* 72, 27–36.

851

852 Jaumot, J., de Juan, A., Tauler, R., 2015. MCR-ALS GUI 2.0: New features and applications.
853 *Chemometrics and Intelligent Laboratory Systems* 140, 1–12.

854

855 Jaumot, J., Gargallo, R., de Juan, A., Tauler, R., 2005. A graphical user-friendly interface for MCR-
856 ALS: a new tool for multivariate curve resolution in MATLAB. *Chemometrics and intelligent*
857 *laboratory systems* 76, 101–110.

858

859 Karkanas, P., Kyparissi-Apostolika, N., Bar-Yosef, O., Weiner, S., 1999. Mineral assemblages in
860 Theopetra, Greece: a framework for understanding diagenesis in a prehistoric cave. *Journal of*
861 *Archaeological Science* 26, 1171–1180.

862

863 Kasdan, A., Chimenti, R.J.L., deNeufville, J.P., 1981. Selective detection of uranium by laser-induced
864 fluorescence: a potential remote-sensing technique. 2: Experimental assessment of the remote sensing
865 of uranyl geologic targets. *Appl. Opt.* 20, 1297–1307.

866

867 Kinnunen, K.A., Ikonen, L., 1991. Opal, a new hydromorphic precipitate type from gravel deposits in
868 southern Finland. *Bulletin of the Geological Society of Finland* 63, 95–104.

869

870 Kumar, K., 2018. Application of Genetic Algorithm (GA) Assisted Partial Least Square (PLS)
871 Analysis on Trilinear and Non-trilinear Fluorescence Data Sets to Quantify the Fluorophores in
872 Multifluorophoric Mixtures: Improving Quantification Accuracy of Fluorimetric Estimations of Dilute
873 Aqueous Mixtures. *Journal of fluorescence* 28, 589–596.

874

875 Mas, S., de Juan, A., Tauler, R., Olivieri, A.C., Escandar, G.M., 2010. Application of chemometric
876 methods to environmental analysis of organic pollutants: a review. *Talanta* 80, 1052–1067.

877

878 McGarry, S. F., Baker, A., 2000. Organic acid fluorescence: applications to speleothem
879 palaeoenvironmental reconstruction. *Quaternary Science Reviews* 19(11), 1087-1101.

880

881 Monger, H.C., Kelly, E.F., 2002. Silica minerals. *Soil mineralogy with environmental applications* 7,
882 611–636.

883

884 Monney, J., 2018. L'art pariétal paléolithique de la grotte aux Points d'Aiguèze: définition d'un
885 dispositif pariétal singulier et discussion de ses implications. *Karstologia* 72, 45–60.

886

887 Monney, J., 2011. *Projet Datation Grottes Ornées : Rapport d'activité 2011. Grotte aux Points*
888 *(Aiguèze). Rapport non publié, Ministère de la Culture, SRA Occitanie, Montpellier.*

889

890 Monney, J., Jaillet, S., 2019. Phases de fréquentations humaines, ornementation pariétale et processus
891 naturels : Mise en place d'un cadre chronologique pour la grotte aux Points d'Aiguèze. *Karstologia* 72,
892 49–62.

893

894 Morwood, M.J., Walsh, G.L., Watchman, A.L., 2010. AMS radiocarbon ages for beeswax and
895 charcoal pigments in north Kimberley rock art. *Rock Art Research: The Journal of the Australian*
896 *Rock Art Research Association (AURA)* 27 (1), 3–8.

897

898 Neymark, L., Paces, J.B., 2013. Ion-probe U–Pb dating of authigenic and detrital opal from Neogene-
899 Quaternary alluvium. *Earth and Planetary Science Letters* 361, 98–109.

900

901 Neymark, L.A., Amelin, Y.V., Paces, J.B., 2000. ^{206}Pb – ^{230}Th – ^{234}U – ^{238}U and ^{207}Pb – ^{235}U
902 geochronology of Quaternary opal, Yucca Mountain, Nevada. *Geochimica et Cosmochimica Acta* 64,
903 2913–2928.

904

905 Nomade, S., Genty, D., Sascó, R., Scao, V., Féruglio, V., Baffier, D., Guillou, H., Bourdier, C.,
906 Valladas, H., Reigner, E., others, 2016. A 36,000-year-old volcanic eruption depicted in the Chauvet-
907 Pont d’Arc Cave (Ardèche, France)? *PloS one* 11(1), e0146621.

908

909 Northup, K.H., Diana, Lavoie, 2001. Geomicrobiology of caves: a review. *Geomicrobiology journal*
910 18, 199–222.

911

912 Ospitali, F., Smith, D.C., Lorblanchet, M., 2006. Preliminary investigations by Raman microscopy of
913 prehistoric pigments in the wall-painted cave at Roucadour, Quercy, France. *J. Raman Spectroscopy*.
914 37, 1063–1071.

915

916 Oster, J.L., Kitajima, K., Valley, J.W., Rogers, B., Maher, K., 2017. An evaluation of paired $\delta^{18}\text{O}$ and
917 $(^{234}\text{U}/^{238}\text{U})_0$ in opal as a tool for paleoclimate reconstruction in semi-arid environments. *Chemical*
918 *Geology* 449, 236–252.

919

920 Othmane, G., Allard, T., Vercouter, T., Morin, G., Fayek, M., Calas, G., 2016. Luminescence of

921 uranium-bearing opals: Origin and use as a pH record. *Chemical Geology* 423, 1–6.

922

923 Perrette, Y., Delannoy, J.-J., Bolvin, H., Cordonnier, M., Destombes, J.-L., Zhilinskaya, E.A.,
924 Aboukais, A., 2000. Comparative study of a stalagmite sample by stratigraphy, laser induced
925 fluorescence spectroscopy, EPR spectrometry and reflectance imaging. *Chemical Geology* 162, 221–
926 243.

927

928 Perrette, Y., Delannoy, J. J., Desmet, M., Lignier, V., Destombes, J. L., 2005. Speleothem organic
929 matter content imaging. The use of a Fluorescence Index to characterise the maximum emission
930 wavelength. *Chemical Geology* 214 (3-4), 193-208.

931

932 Pons-Branchu, E., Bourrillon, R., Conkey, M.W., Fontugne, M., Fritz, C., Gárate, D., Quiles, A.,
933 Rivero, O., Sauvet, G., Tosello, G., 2014. Uranium-series dating of carbonate formations overlying
934 Paleolithic art: interest and limitations. *Bulletin de la Société préhistorique française* 211–224.

935

936 Quiers, M., Perrette, Y., Chalmin, E., Fanget, B., Poulénard, J., 2015. Geochemical mapping of
937 organic carbon in stalagmites using liquid-phase and solid-phase fluorescence. *Chemical Geology* 411,
938 240-247.

939

940 Quiles, A., Fritz, C., Alcaide, M.Á.M., Pons-Branchu, E., Torti, J.L.S., Tosello, G., Valladas, H.,
941 2015. Chronologies croisées (C-14 et U/Th) pour l'étude de l'art préhistorique dans la grotte de Nerja:
942 méthodologie. Presented at the *Sobre rocas y huesos: las sociedades prehistóricas y sus*
943 *manifestaciones plásticas*, UCO Press. Editorial de la Universidad de Córdoba, pp. 420–427.

944

945 Sadier, B., 2013. 3D et géomorphologie karstique : La grotte Chauvet et les cavités des Gorges de
946 l'Ardèche (Thèse). Université de Savoie, Le-Bourget-Du-Lac.

947

948 Savitzky, A., Golay, M.J.E., 1964. Smoothing and Differentiation of Data by Simplified Least
949 Squares Procedures. *Analytical Chemistry*. 36, 1627–1639.

950

951 Shao, Q.-F., Pons-Branchu, E., Zhu, Q.-P., Wang, W., Valladas, H., Fontugne, M., 2017. High
952 precision U/Th dating of the rock paintings at Mt. Huashan, Guangxi, southern China. *Quaternary*
953 *Research* 88, 1–13.

954

955 Valladas, H., Pons-Branchu, E., Dumoulin, J.P., Quiles, A., Sanchidrián, J.L., Medina-Alcaide, M.Á.,
956 2017. U/Th and ¹⁴C Crossdating of Parietal Calcite Deposits: Application to Nerja Cave (Andalusia,
957 Spain) and Future Perspectives. *Radiocarbon* 59, 1955–1967.

958

959 Van Beynen, P., Bourbonniere, R., Ford, D., Schwarcz, H., 2001. Causes of colour and fluorescence in
960 speleothems. *Chemical Geology* 175 (3-4), 319-341.

961

962 Watchman, A., 2000. A review of the history of dating rock varnishes. *Earth-Science Reviews* 49,
963 261–277.

964

965 Watchman, A., 1990. What are silica skins and how are they important in rock art conservation?
966 *Australian Aboriginal Studies* 1, 21–29.

967

968 Zhang, X., Tauler, R., 2013. Application of multivariate curve resolution alternating least squares
969 (MCR-ALS) to remote sensing hyperspectral imaging. *Analytica chimica acta* 762, 25–38.

970

971 Zielinski, R.A., 1982. Uraniferous opal, Virgin Valley, Nevada: Conditions of formation and
972 implications for uranium exploration. *Journal of Geochemical Exploration* 16, 197–216.

973

974 Zielinski, R.A., 1980. Uranium in secondary silica; a possible exploration guide. *Economic Geology*
975 75, 592–602.